Artificial Intelligence Research and Applications (AIra)
https://www.ijaira.org/ Online ISSN: 3108-3889
K.N. Khallouf and H. Benbouhenni, Vol. 2, No. 3, September, 2026 Research Article

Fuzzy Logic–Based Control for Photovoltaic Systems with Integrated Energy Storage

Khaoula Nermine Khallouf*, Habib Benbouhenni**‡

* Department of Electrical Engineering, Laboratory of mod ERNA, Mentouri Univ. of Constantine 1, Constantine, Algeria.

** Department of Electrical Engineering, Faculty of Technology, Hassiba Benbouali University of Chlef, B.P 78C Ouled Fares, Chlef 02180, Algeria.

(khaoula-nermine.khallouf@student.umc.edu.dz, h.benbouhenni@univ-chlef.dz)

‡ Corresponding Author: Habib Benbouhenni, Hassiba Benbouali University of Chlef, h.benbouhenni@univ-chlef.dz.

Received: 08.11.2025, Revised: 12.04.2026, Accepted: 05.05.2026

Abstract- The application of fuzzy logic control (FLC) to a photovoltaic (PV) system with an energy storage solution aims to enhance the efficiency, reliability, and stability of renewable energy generation. In such systems, solar panels convert sunlight into electrical power, while a storage device—typically a battery—stores excess energy for later use or grid support. Because PV output fluctuates due to changing weather conditions and varying solar irradiance, maintaining optimal energy flow and battery management becomes complex. FLC method provides an effective solution by mimicking human decision-making through a set of linguistic rules rather than relying on precise mathematical models. This allows the controller to handle the nonlinear and uncertain behaviour of PV systems. The FLC technique can dynamically regulate parameters such as the duty cycle of DC–DC converters, battery charge/discharge rates, and power balance between the PV array, the battery, and the load or grid. Compared with conventional control methods (e.g., PID control), FLC method offers better adaptability and robustness under rapidly changing environmental conditions. Simulation and experimental results reported in research show that FLC approach improves system performance by achieving smoother power output, faster response to irradiance variations, and prolonged battery lifespan through optimized energy management. In summary, integrating FLC method into PV systems with storage enhances energy conversion efficiency, system stability, and overall reliability—making it a valuable method for modern smart grids and sustainable energy applications.

Keywords: Fuzzy logic, photovoltaic system**,** DC–DC converters**,** renewable energy generation**,** energy storage.

1. Introduction

Fuzzy logic (FL), first introduced by Lotfi A. Zadeh in 1965, is an extension of classical Boolean logic, designed to handle approximate rather than fixed and precise reasoning [1]. Unlike traditional binary logic, where variables must take values of either 0 or 1, FL method allows variables to have truth values ranging from 0 to 1. This capability makes it particularly suitable for systems involving uncertainty, inaccuracy, or complex nonlinear relationships, which are common characteristics in renewable energy systems [2].

In renewable energy applications, FL controllers (FLCs) are increasingly used in decision-making, control, and optimization tasks, due to their ability to mimic human reasoning and adapt to changing environmental conditions [3]. For example, FLC method has been used in maximum power point tracking (MPPT) for photovoltaic (PV) power systems [4], wind turbine control [5], energy management in hybrid renewable energy systems [6], and load forecasting [7].

Cite this article as: K.N. Khallouf and H. Benbouhenni, "Fuzzy Logic–Based Control for Photovoltaic Systems with Integrated Energy Storage," *Artificial Intelligence Research and Applications (AIra)*, Vol. 2, No. 3, pp. 156–166, September, 2026, https://doi.org/10.20508/qtrxhx79.

Each of these applications offers distinct advantages. FLCs do not require a precise mathematical model of the system, making them robust to parameter variations and measurement noise [8]. They can also efficiently handle nonlinear interference in wind and solar power conversion processes and adapt to rapidly changing weather conditions. Furthermore, fuzzy systems are relatively easy to integrate with other control algorithms, such as neural networks or genetic algorithms [9, 10], forming powerful hybrid intelligent controllers.

However, there are also drawbacks. Designing an effective FL system often relies on expert knowledge to define membership functions and rules, which can be subjective and time-consuming [11]. FL systems may require extensive tuning for varying operating conditions, and their performance may deteriorate when applied to systems beyond the scope of the initial design. In addition, compared to model-based control methods, FL may sometimes lack transparency and interpretability, especially in large-scale applications [12]. In general, FL provides a flexible and effective framework for managing uncertainty and improving the performance of renewable energy systems [13]. Its adaptability and robustness make it a valuable tool for optimizing energy generation and consumption, although careful design and validation are essential to overcome its inherent limitations [14].

Combining FL method with advanced control strategies, such as direct power control (DPC) [15], space vector control (or space vector)/switch table control (STC) [16], field-oriented control (FOC) [17], slide mode control (SMC) [18], and backstepping control (BC) [19], enhances the overall robustness, adaptability, and dynamic performance of electric motor and power converter systems. FL method can be incorporated as an intelligent supervisor or adaptive tuner that adjusts control gains, switching thresholds, or reference parameters in real time, compensating for modeling uncertainty, nonlinearity, and external disturbances. In DPC method and self-tuning control (STC) systems, fuzzy rule sets facilitate switching and reduce torque and flux ripples. When applied with a FOC system, fuzzy inference improves the accuracy of speed and current loops under varying load conditions. In SMC and BC techniques, FL method can mitigate the effects of oscillation and simplify the design of control laws by replacing complex mathematical models with rule-based approximations. Overall, the hybridization of FL method with these nonlinear control techniques achieves a more flexible and error-resistant control architecture, suitable for high-performance electric drives and renewable energy systems.

Photovoltaic (PV) systems, which convert sunlight directly into electricity using semiconductor materials, have become one of the most promising and fastest-growing renewable energy technologies in the modern world [20]. Their importance in the energy and industrial sectors stems from the global need to reduce dependence on fossil fuels, lower greenhouse gas emissions, and promote sustainable energy solutions [21]. PV power systems offer many advantages, including clean and quiet operation, low maintenance and installation requirements, and the ability to deploy in diverse environments-from rooftops and remote rural areas to large-scale solar farms and industrial facilities [22]. Furthermore, advances in PV materials, power electronics, and energy storage have improved their efficiency and integration into smart grids and hybrid energy systems. However, despite their advantages, PV power systems face several drawbacks and challenges [23]. Their energy production is inherently intermittent and weather-dependent, leading to fluctuations in power output and necessitating reliable energy storage or backup systems. While initial installation costs may decrease over time, they remain relatively high compared to conventional energy sources, particularly in developing regions [24]. In addition, issues related to energy conversion efficiency, land use for large installations, and the environmental impact of PV panel manufacturing and disposal must be addressed. In the industrial and commercial sectors, PV systems are widely used to power manufacturing plants, telecommunications, agricultural irrigation, and remote monitoring systems [24]. Key challenges hindering widespread adoption include limited energy storage technologies, grid integration difficulties, and the need for supportive policies and infrastructure. Overcoming these obstacles will be essential to realizing the full potential of PV systems as a cornerstone of a sustainable and resilient energy future [25].

This work addresses the enhancement of performance, stability, and energy efficiency in PV power conversion and management by proposing an intelligent control strategy based on a FLC method. The main contribution of this study is the design, implementation, and comprehensive simulation of an FLC capable of effectively regulating power flow between the PV array, the energy storage system, and the load under varying operating conditions such as changes in irradiance, temperature, and load demand. In addition, a systematic comparative analysis with a conventional PI controller is conducted to highlight the advantages of the proposed approach. This comparison focuses on key performance indicators, including reference tracking accuracy, reduction of current and power ripples, minimization of response time, overshoot and undershoot in DC-link voltage, and mitigation of THD in the current. The results demonstrate that the proposed FLC provides superior robustness, adaptability, and dynamic performance, particularly in handling the nonlinearities and uncertainties inherent in PV systems. Overall, the study confirms the effectiveness of the proposed control strategy in improving system efficiency, reducing energy losses, and enhancing the reliability of hybrid PV systems with energy storage.

The main objectives achieved in this work are summarized as follows:

- Maintaining the stability of the DC-link voltage under varying operating conditions.
- Improving the charging and discharging performance of the energy storage unit.
- Ensuring continuous and reliable power supply despite fluctuations in irradiance and load.
- Reducing current and power ripples and minimizing harmonic distortion.
- Enhancing dynamic response by reducing rise time, overshoots, and undershoots.

- Increasing overall energy efficiency and reducing system losses.
- Demonstrating the superiority of the FLC approach over the conventional PI controller.

The manuscript has five distinct sections. Following the introduction, the modelling and design of the microgrid system proposed in this paper are presented. Section three details the control approach applied to the microgrid system, highlighting its key advantages over traditional methods. Section four presents the results obtained from both the traditional and the designed approaches, including numerical data. In the fifth section, the most important conclusions obtained from this work are listed, along with a proposal for future work as a complement to this work

2. Design and Modelling of the Microgrid (MG) System

This paper is devoted to the study of the MG system associated to the PV system. The form of the designed structure is presented in Figure 1. Relying on this system allows for a reduction in the use of non-renewable resources, thus mitigating the effects of global warming. Furthermore, its use reduces the costs of energy production and consumption. This system can be installed on rooftops, creating several practical solutions that significantly contribute to the development of the electrical energy sector. This system, designed in this study, is highly effective in isolated and remote areas, as its adoption greatly reduces power transmission lines and the damage these lines cause to arable land.

This structure involves the connection of all converter systems via a common DC bus. The inspected system consists of a PV energy system, and a battery energy storage system (ESS). The PV system consists of a PV array associated with the DC-DC-BC, and the battery-ESS is composed of the BS and the DC/DC reversible chopper. All these converter systems are linked through a common DC bus to the coupling point (PCC) by the Multifunctional voltage source inverter (MFVSI), feeding a nonlinear load.

To extract the ME conversion from the system, a comparative work between two types of control, traditional PI and intelligent artificial FLC, the maximum power point tracking (MPPT) based on PI control and the FLC technique were applied in the control at each converter in the system, and at the MFVSI inverter to get better the power quality at the PCC.

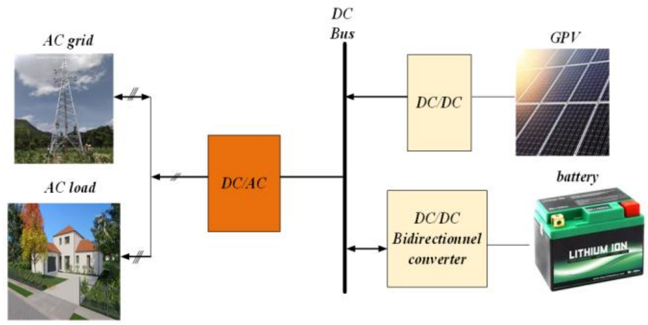

Fig. 1. The designed power system.

2.1. PV System Model

A solar cell is a device that converts solar energy into electricity using the PV effect, which is closely related to the P-N junction of semiconductors. In this study, a PV cell model based on the static behaviour of a conventional P-N junction diode is used [26]. The electrical model includes a current source in parallel with a diode, a shunt resistance (r_{sh}), and a series resistance (r_s). The shunt resistance represents current leakage and parasitic currents due to material defects or impurities, while the series resistance accounts for the internal resistance of the semiconductor and its connections. It is important to arrange the modules in series, parallel, or a mixed configuration to form a PV array capable of delivering appropriate voltage and power levels, potentially reaching several kilowatts. The equivalent circuit is shown in Figure 2 [23].

The output current of the PV array is mathematically expressed as [21]:

$$i_{pv} = N_p I_{ph} - N_p I_0 \cdot \left[exp\left(\frac{q}{N_s N_p \gamma K T} \left(V_{pv} + \frac{N_s}{N_p} r_s \, i_{pv} \right) \right) - 1 \right] - \frac{\left(V_{pv} + \frac{N_s}{N_p} r_s \, i_{pv} \right)}{\frac{N_s}{N_p} r_{sh}} \quad (1)$$

2.2. Modelling of the DC-DC Converter in the PV System

The DC-DC boost converter is designed to increase the voltage supplied by the PV array to an optimal level, thereby maximizing energy production [27]. A capacitor is typically placed between the generator and the boost converter to reduce high-frequency harmonics. Figure 3 shows a schematic diagram of the DC-DC boost converter used in the system under study. This type was chosen for its simplicity and ease of implementation. Furthermore, this converter is easy to control, making it a superior choice.

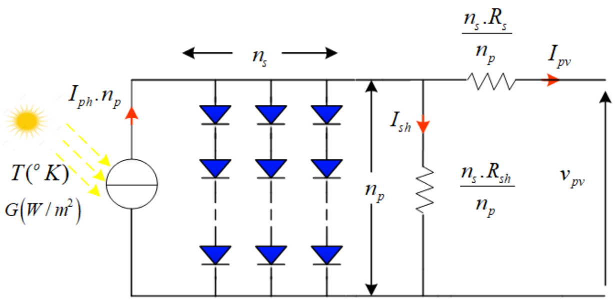

Fig. 2. Equivalent circuit of the PV array.

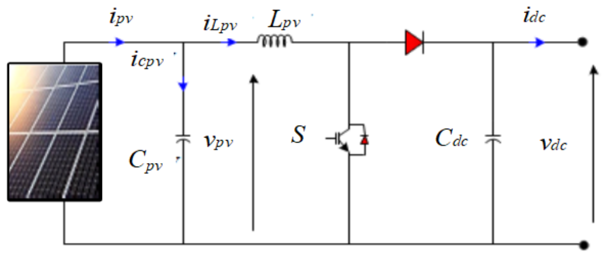

Fig. 3. Equivalent circuit of the PV array.

The differential equations governing the dynamics of the input voltage and the current through the inductor are expressed as follows [28]:

$$\begin{cases} C_{pv}\dfrac{dv_{pv}}{dt} = i_{pv} - i_L \\ \dfrac{di_L}{dt} = \dfrac{1}{L_{pv}} v_{pv} - (1-D)\dfrac{1}{L_{pv}} v_{dc} \end{cases} \quad (2)$$

Here, v_{pv} and i_{pv} represent the voltage and current generated by the PV array, respectively, while i_L denotes the current flowing through the inductor of the DC-DC converter. v_{dc} refers to the DC bus voltage, D is the duty cycle, and C_{PV} and L_{PV} are the electrical parameters of the boost converter

2.3. *Mathematical Models of Batteries*

Although Li-ion batteries are relatively expensive, they offer outstanding performance due to their high energy density, output voltage, and low self-discharge rate, making them especially suitable for microgrids [29]. This is illustrated by the Berger model, shown in the Figure 4.

The mathematical model of the battery in charge/discharge mode is given in [30]:

- Charging mode:

$$\begin{aligned} V_{dis} &= E_0 - K\frac{Q}{Q-it}(i_t) - R_{int} i + A e^{-B\times t} - K\frac{Q}{Q-it} i^* \\ &= E_0 - \underbrace{R_{int} i}_{V_{ohm}} - \underbrace{K\frac{Q}{Q-it}\left(i_t + i^*\right)}_{V_{pol}} + V_{exp} \end{aligned} \quad (3)$$

- Discharging mode:

$$\begin{aligned} V_{ch} &= E_0 - K\frac{Q}{Q-it}(i_t) - R_{int} i + A e^{-B\times t} - K\frac{Q}{it-0.1Q} i^* \\ &= E_0 - \underbrace{R_{int} i}_{V_{ohm}} - \underbrace{K\frac{Q}{Q-it}\left(\frac{Q}{Q-it} i_t + K\frac{Q}{it-0.1Q} i^*\right)}_{V_{pol}} + V_{exp} \end{aligned} \quad (4)$$

The battery output voltage (V_b) is defined by the discharge voltage (V_{dis}) and the charge voltage (V_{ch}). (E_o) represents the reference voltage during charging. The maximum battery capacity is denoted by *Q* (Ah), and it includes a polarization constant *K* (V/Ah), internal resistance R_{int} (Ω), and discharge current i_b (A).

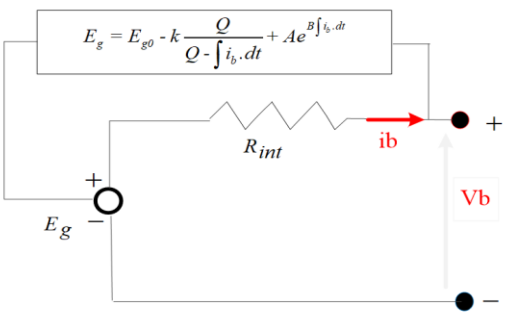

Fig. 4. Equivalent model of a battery.

The instantaneous discharge current is represented by (i_b × *t*), and the filtered discharge current is noted as i_b^* (A). Finally, *A* refers to the amplitude of the exponential zone (V), and *B* is the inverse time constant for this exponential zone (Ah^{-1}).

The state of charge (SOC) of a battery can be estimated based on the discharge current and the battery capacity:

$$SOC = SOC_0 - \frac{1}{Q}\int idt \quad (5)$$

2.4. *Mathematical Model of the Bidirectional DC-DC Converter in the Storage System*

For energy conversion in a battery ESS, a bidirectional flow of electrical energy is required. To achieve this, a bidirectional DC-DC current converter has been integrated into the control system [31]. The corresponding schematic of the converter is shown in Figure 5.

The following equations describe the dynamic model of the BESS (Battery Energy Storage System).

$$\begin{cases} \dfrac{di_b}{dt} = \dfrac{V_b - i_b R_b - D_b . v_{dc}}{L_b} \\ \dfrac{dv_{dc}}{dt} = \dfrac{1}{C_{dc}}\left(V_b - i_b D_b - i_{dc}\right) \end{cases} \quad (6)$$

2.5. *Mathematical Model of the AC Side*

Figure 6 shows the equivalent electrical diagram of the AC side, which includes a MFVSI, a nonlinear load, and an AC grid.

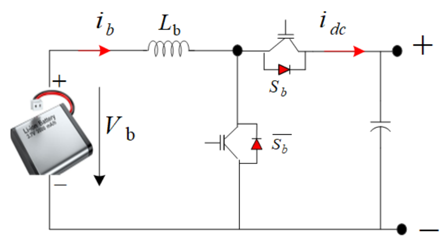

Fig. 5. Topologies of the bidirectional converter.

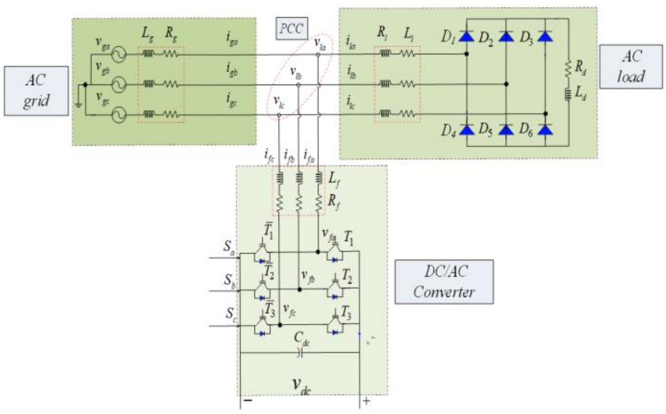

Fig. 6. Equivalent electrical diagram of the AC side.

The equation linking the grid-side current and voltage is derived using Kirchhoff's laws applied to the above circuit and can be expressed as follows:

$$\frac{di_{gabc}}{dt} = \frac{1}{L_f} v_{gabc} - \frac{R_g}{L_g} i_{gabc} + \frac{1}{L_g} v_{\ell_{abc}} \tag{7}$$

The load consists of a three-phase diode rectifier (Graetz bridge), connected to the grid through a line impedance (*Z*), supplying an inductive load (*R* and *L*), as shown in Figure 6. The inductance (*L*) varies between 1–10% of its nominal value and is expressed as:

$$L_\ell = \frac{v_g}{\omega . i_{\ell a}} \tag{8}$$

with:

$$i_{\ell a} = \sqrt{\frac{3}{2}} i_d \tag{9}$$

The behaviour of the APF currents in a three-phase reference frame is described by the following system of equations [32]:

$$\begin{cases} \dfrac{di_{f_{abc}}}{dt} = -\dfrac{R_f}{L_f} i_{fabc} + \dfrac{1}{L_f} v_{f_{abc}} - \dfrac{1}{L_f} v_{\ell abc} \\ \dfrac{dv_{dc}}{dt} = \dfrac{1}{C_{dc}} i_{dc} - S_{abc} i_{fabc} \end{cases} \tag{10}$$

The expressions of the inverter's phase (line-to-neutral) voltages based on the switching states (S_a, S_b, S_c) are given by the following equation:

$$\begin{cases} v_{f1} = \dfrac{V_{dc}}{3}(2S_a - S_b - S_c) \\ v_{f2} = \dfrac{V_{dc}}{3}(2S_a - S_b - S_c) \\ v_{f3} = \dfrac{V_{dc}}{3}(2S_c - S_b - S_a) \end{cases} \tag{11}$$

3. The Proposed Control Method of Converter of the MG

FL operators are mathematical functions defined on the interval [0, 1] that allow the combination of degrees of truth. They extend the classical Boolean operators "AND", "OR", and "NOT".

The intersection of two fuzzy sets A and B is defined as:

$$\mu_{A \cap B}(x) = min\left(\mu_A(x), \mu_B(x)\right) \tag{12}$$

The union of two fuzzy sets A and B is defined as:

$$\mu_{A \cup B}(x) = max\left(\mu_A(x), \mu_B(x)\right) \tag{13}$$

The complement of a fuzzy set is characterized by the following membership function:

$$\mu_{\bar{A}}(x) = 1 - \mu_A(x) \tag{14}$$

The fuzzy controller features a modular architecture consisting of three main blocks, as illustrated in Figure 7. These modules are: fuzzification, inference module, and defuzzification.

According to Figure 7, the FLC system consists of the following key components:

- Acquisition: Measurement of the output using an analog/digital sensor.
- Processing: Calculation of the error (e) and its variation (Δe), followed by normalization using the gains Ke, KΔe, and KΔu.
- Fuzzy Core: Includes the FL rule base and the defuzzification process (conversion to a numerical control value).
- Control Generation: Integration of Δu (summation) and application of the final control law.

The form of the control law is given by:

$$u\,(k+1) = u_k\,(k) + K_{\Delta u}.\Delta u(k) \tag{15}$$

Where *KΔu* and *Δu(k)* represent the gain associated with the control signal *u(k+1)* and the variation in the control action, respectively.

The error (*e*) and its variation (Δ*e*) are defined as follows:

$$\begin{cases} E_e = K_e.e \\ E_{\Delta e} = K_{\Delta e}.\Delta e \end{cases} \tag{16}$$

Where, *Ke* and *KΔe* are the normalization factors, which play a critical role in the performance of the control system.

The membership functions were designed using a heuristic approach based on the system dynamics and control objectives. Specifically, symmetrical triangular and trapezoidal membership functions were adopted due to their simplicity and effectiveness, ensuring full coverage of the input (error and change of error) and output domains. The ranges of these functions were selected according to the expected operating limits of the system and have now been explicitly illustrated in the manuscript.

The proposed FLC employs a total of 49 fuzzy rules (7×7), constructed based on expert knowledge and the desired control behavior linking the error and its variation to the control action. These rules are now clearly presented in the form of a rule table for improved clarity and reproducibility.

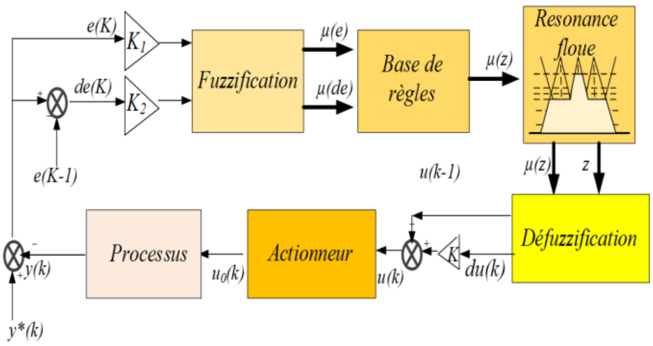

Fig. 7. Structure of the FLC.

Regarding the normalization gains (Ke, KΔe, KΔu), they were initially selected based on the system's operating range to properly scale the input and output variables into normalized fuzzy domains.

Subsequently, these gains were fine-tuned through an iterative trial-and-error procedure using simulation results, with the objective of achieving optimal performance in terms of fast response, minimal overshoot, and reduced steady-state error (SSE). The final selected values are now reported in the revised manuscript.

Figure 8 represents the membership functions used in this work to embody the mysterious controller.

Table 1 shows the number of rules used in this paper. Seven rules were used in each entry, resulting in a total of 49 rules, where Negative Large (NL), Negative Medium (NM), Negative Small (NS), Approximately Zero (EZ), Positive Small (PS), Positive Medium (PM), and Positive Large (PL).

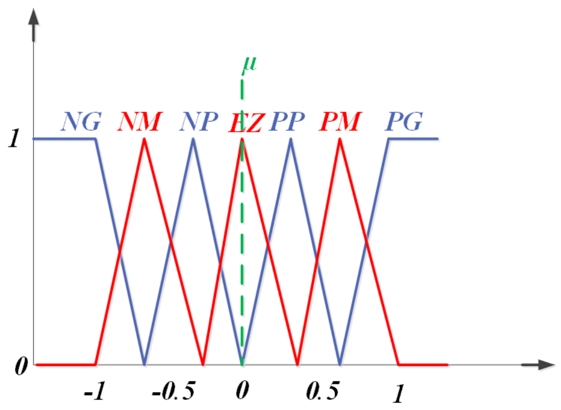

Fig. 8. Membership function of a linguistic variable with seven classes.

Table 1. Fuzzy rules.

Δe \ e	NG	NM	NP	EZ	PP	PM	PG
NG	NG	NG	NG	NG	NM	NP	EZ
NM	NG	NG	NG	NM	NP	EZ	PP
NP	NG	NG	NM	NP	EZ	PP	PM
EZ	NG	NM	NP	EZ	PP	PM	PG
PP	NM	NP	EZ	PP	PM	PG	PG
PM	NP	EZ	PP	PM	PG	PG	PG
PG	EZ	PP	PM	PG	PG	PG	PG

3.1. Application of the FLC on the DC Side

The system requires the control of: PV power (*Ppv*), and battery current. To achieve this control FLCs are implemented—two dedicated to the PV system, and one for the battery ESS.

The normalized errors are defined as follows:

$$e_{P_{pv}}(K) = K_{e_{P_{pv}}} \frac{(P_{pv}(K+1) - P_{pv}(K))}{(v_{pv}(K+1) - v_{pv}(K))}$$
$$e_{i_b}(K) = K_{e_{i_b}} (i_b^*(K) - i_b(K)) \quad (17)$$

where, *Ke*, *KΔe*, and *KΔu* are the normalization gains for the error signals.

The variations of these errors are given by:

$$\Delta e_{P_{pv}}(K) = K_{\Delta e_{P_{pv}}} (e_{P_{pv}}(K+1) - e_{P_{pv}}(K))$$
$$\Delta e_{i_b}(K) = K_{\Delta e_{i_b}} (i_b^*(K) - i_b(K)) \quad (18)$$

where *KΔe* values represent the gains used for normalizing the error changes.

The outputs of the FLCs are given by:

$$\overline{\Delta D_{pv}} = \frac{\sum_{m=1}^{N=49} D_{pv,m}\,\mu(D_{pv,m})}{\sum_{m=1}^{N=49} \mu(D_{pv,m})} \quad (19)$$

$$\overline{\Delta D_b} = \frac{\sum_{m=1}^{N=49} D_{b,m}\,\mu(D_{b,m})}{\sum_{m=1}^{N=49} \mu(D_{b,m})} \quad (20)$$

3.2. Application of the FLC on the AC Side

To achieve the goals, dedicated control architecture is implemented, consisting of three FLCs:

- The v_{dc} controller ensures the energy stability of the DC bus.
- The P_g controller regulates the flow of active power.
- The Q_g controller manages reactive power compensation.

The normalized errors are defined as:

$$e_{v_{dc}}(K) = K_{e_{v_{dc}}} (v_{dc}^*(K) - v_{dc}(K))$$
$$e_{p_g}(K) = K_{e_{p_g}} (p_g^*(K) - p_g(K))$$
$$e_{q_g}(K) = K_{e_{q_g}} (q_g^*(K) - q_g(K)) \quad (21)$$

Where, Ke_{vdc}, Ke_{Pg}, and Ke_{Qg} are the normalization gains for each respective variable.

The variations of these errors are given by:

$$\begin{aligned}\Delta e_{v_{dc}}(K) &= K_{\Delta e_{v_{dc}}}(e_{v_{dc}}(K) - e_{v_{dc}}(K-1)) \\ \Delta e_{p,f\alpha}(K) &= K_{\Delta e_{p_g}}(e_{p,f\alpha}(K) - e_{q_g}(K-1)) \\ \Delta e_{q_g}(K) &= K_{\Delta e_{q_g}}(e_{q,f\beta}(K) - e_{q_g}(K))\end{aligned} \quad (22)$$

Where, $K\Delta e\_v_{dc}$, $K\Delta e\_P_g$, and $K\Delta e\_Q_g$ are the corresponding gains.

The FLC outputs are given by:

$$\overline{\Delta p_g} = \frac{\sum_{i=1}^{N=49} v_{dc,m}\,\mu(v_{dc,m})}{\sum_{i=1}^{N=49} \mu(v_{dc,m})} \quad (23)$$

$$\overline{\Delta v_{f\alpha}} = \frac{\sum_{m=1}^{N=49} p_{g,m}\,\mu(p_{g,m})}{\sum_{m=1}^{N=49} \mu(p_{g,m})} \quad (24)$$

$$\overline{\Delta v_{f\beta}} = \frac{\sum_{m=1}^{N=49} q_{g,m}\,\mu(q_{g,m})}{\sum_{m=1}^{N=49} \mu(q_{g,m})} \quad (25)$$

The APF control voltages (v_{fd} and v_{fq}) are obtained using the following equation:

$$\begin{cases} v_{fd}^{*} = v_{\ell d}^{*} + R_f i_{fd} + L_f \dfrac{di_{fd}}{dt} + L_f \omega i_{fq} \\ v_{fq}^{*} = v_{\ell q}^{*} + R_f i_{fq} + L_f \dfrac{di_{fq}}{dt} - L_f \omega i_{fd} \end{cases} \quad (26)$$

Once the APF control voltages are obtained, the DPC-SVM (direct power control with space vector modulation) strategy is applied, using a constant switching frequency. The DPC approach is illustrated in Figure 9.

The designed approach relies on using the SVM approach to generate the necessary pulses. SVM method is an advanced control strategy used in power electronics, particularly for driving three-phase inverters. Its working principle is based on representing the three-phase output voltages as a single rotating vector in a two-dimensional plane (α-β reference frame). By selecting and timing the appropriate switching states of the inverter, SVM approximates this reference vector within each sampling period using combinations of adjacent active vectors and zero vectors.

This approach allows more efficient utilization of the DC bus voltage compared to traditional sinusoidal Pulse Width Modulation (PWM). One of the main advantages of SVM over PWM is its ability to achieve a higher output voltage (up to about 15% more), which improves the overall performance of the inverter. Additionally, SVM produces lower harmonic distortion, leading to smoother motor operation and reduced losses. It also offers better control over switching sequences, which can minimize switching losses and optimize thermal performance.

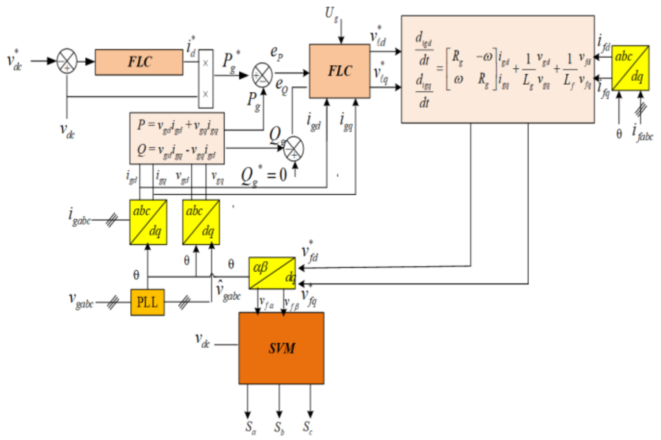

Fig. 9. Functional diagram of the proposed FLC-DPC-SVM strategy.

Adopting a design-based approach based on the SVM strategy allows for significant improvements in energy quality and operational performance. However, using the SVM approach increases the complexity of the design approach.

The proposed FLC-DPC-SVM strategy exhibits higher computational complexity compared to the conventional DPC-PI approach due to the integration of both FLC method and SVM approach. In the DPC-PI method, the control structure relies primarily on proportional–integral regulators and hysteresis-based switching, which involve relatively simple arithmetic operations and straightforward implementation.

In contrast, the FLC-DPC-SVM scheme requires additional processing steps, including fuzzification of input variables, rule base evaluation, and defuzzification, all of which increase the computational burden. Moreover, the incorporation of SVM introduces further calculations for sector identification, vector selection, and duty cycle determination within each sampling period.

Despite this increased complexity, the FLC-DPC-SVM approach offers superior performance in terms of reduced torque and flux ripples, improved dynamic response, and lower harmonic distortion, which can justify the added computational cost in modern digital control platforms with sufficient processing capability.

4. Result and Discussion

The designed approach is tested using MATLAB, with the results compared to the existing PI controller approach. Performance is evaluated in terms of ripple, reference tracking, THD of current, steady-state error, and response time.

The system parameters used in this work are listed in Table 2.

Table 3 represents some of the key details of the simulations in the MATLAB software that were used. Graphical results are presented in Figure 10, while numerical results are listed in Tables 4.

Table 2. Parameters of the studied system.

Li ion battery system	
Battery converter capacitance	4 mF
Battery converter resistance	0.05 Ω
Battery	100 Ah
Battery converter inductance	1 mH
Nominal voltage (V_n)	400 V
Nonlinear load	
Inductance	83.2 mH
Resistance	51.64 Ω
PV array	
Voltage at maximum power point (V_{mp})	34.5 V
Maximum power (P_{mp})	150 W
Open circuit voltage (V_{oc})	43.5 V
Solar irradiation reference (G_{ref})	1000 W/m²
Short circuit current (I_{sc})	4.35 V
Cell temperature reference(T_{ref})	25 °C
Current at maximum power point (I_{mp})	4.35 A

Table 3. Some key details of simulation processes in software.

Parameter	Symbol	Value	Unit
Controller Sampling Frequency	*fs*_ctrl	10	kHz
Inverter Switching Frequency	*fs*_sw	20	kHz
Grid Voltage	*V*_grid	230	V
Grid Frequency	*f*_grid	50	Hz
Grid Resistance	*R*_grid	0.1	Ω
Grid Inductance	*L*_grid	1.5	mH
Initial State of Charge	SOC_init	60	%
Minimum State of Charge	SOC_min	20	%
Maximum State of Charge	SOC_max	80	%
Nominal Capacity	C_b	100	Ah
Module Voltage	V_b	12	V
Number of Series Modules	N_b	33	—
Nominal Battery Voltage	V_{bat}	400	V
Nominal Battery Power	P_b	5	kW

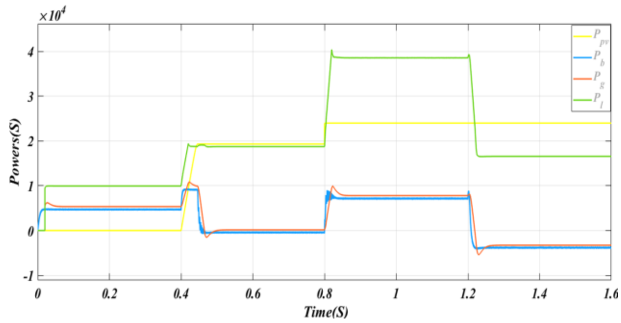

(a) Powers.

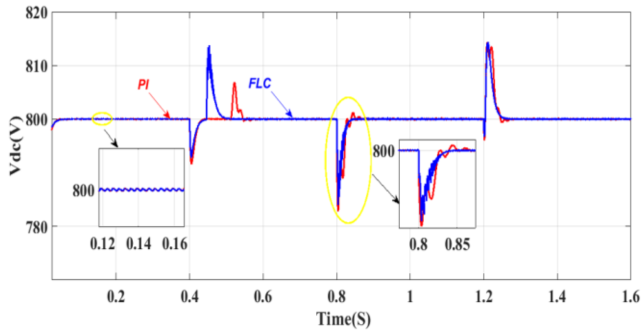

(b) DC link voltage.

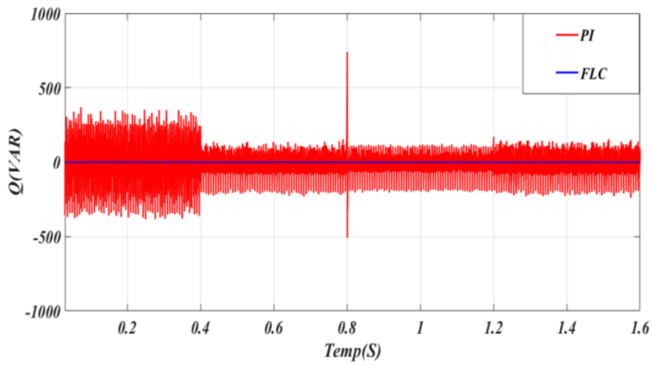

(c) Reactive power.

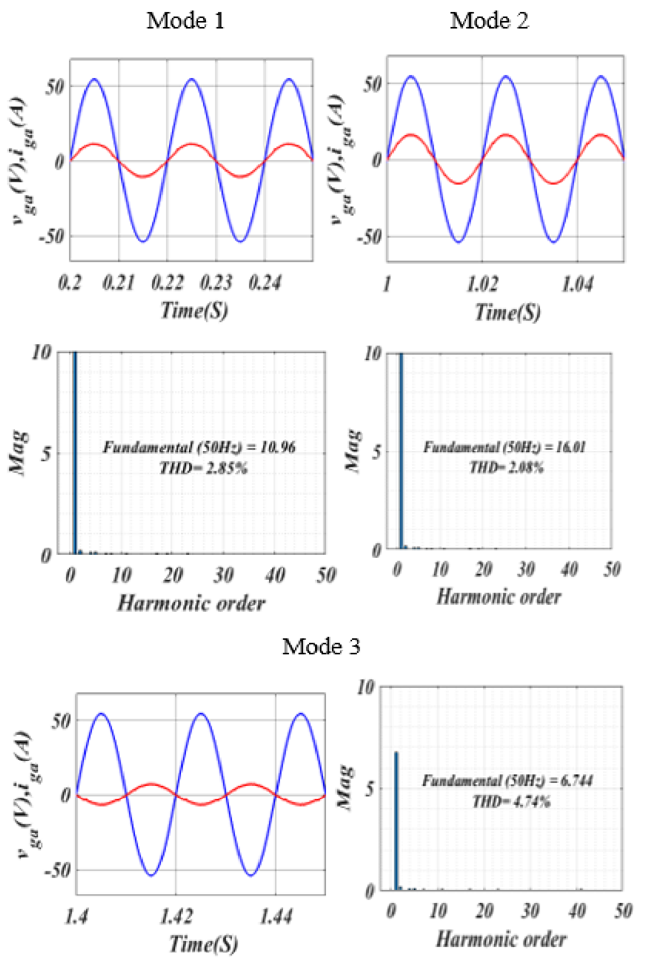

(d) THD of current (PI).

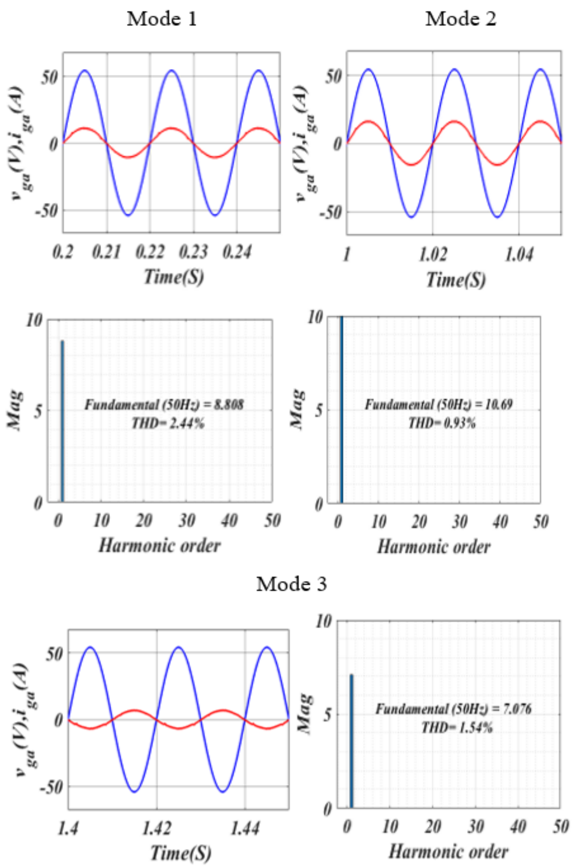

(e) THD of current (FLC).

Fig. 10. The graphical results.

Table 4. The THD values for the both techniques

Modes	PI %	FLC %	Ratios (%)
Mode 1	2.85	2.44	14
Mode 2	2.08	0.93	55
Mode 3	4.74	1.59	66

Table 5 compares the performance of a conventional PI controller and a FLC method for regulating DC link voltage. The results clearly demonstrate that the FLC technique delivers superior performance in both transient and steady-state conditions. Voltage ripple decreased from 0.20 V (PI) to 0.08 V (FLC), representing a 60% improvement, indicating smoother voltage regulation and reduced steady-state fluctuations. Bypassing was reduced by 25%, confirming improved response to transient states and reduced stress on the system. Furthermore, the FLC method achieves a faster response time of 0.04 seconds compared to 0.07 seconds for the PI controller, reflecting a 43% improvement in dynamic performance. The SSE also decreased significantly from 0.12 V to 0.055 V, demonstrating a 58% improvement in steady-state accuracy. Overall, the FLC outperforms the PI controller in all evaluated parameters, providing faster, more stable and more accurate DC link voltage control, thus proving its effectiveness and robustness for demanding electronics applications.

Table 5. The numerical results for the DC link voltage

Parameters	PI	FLC	Ratios (%)
Ripples (V)	0.2	0.08	60
Overshoot (%)	0.8	0.6	25
Response time (s)	0.07	0.04	43
SSE (V)	0.12	0.055	58

Tables 4 and 5 summarize the comparative performance of a conventional PI controller and a FLC in regulating DC-link voltage and reducing harmonic distortion. The results clearly indicate that the FLC offers superior performance in all evaluated parameters. As shown in Table 5, the FLC method achieves lower voltage ripple (0.08 V) compared to the PI controller (0.20 V), representing a 60% reduction. Voltage overshoot is also reduced by 25%, and response time decreases from 0.07 seconds to 0.04 seconds, demonstrating a 43% faster transient response. Furthermore, the SSE is reduced by 58%, indicating more precise voltage regulation and enhanced system stability. Regarding power quality, Table 4 shows that the FLC significantly reduces THD in all operating modes. The THD improvement ranges from 14% in Mode 1 to 66% in Mode 3, confirming the FLC's ability to maintain a cleaner, more sinusoidal output waveform, even under nonlinear or dynamic conditions. Overall, these results demonstrate the superiority of the FLC over the conventional FLC by providing faster response times, lower steady-state error, reduced voltage ripple, and significantly improved harmonic performance. Therefore, the FLC offers a more robust and efficient control solution for regulating DC link voltage and improving overall system performance.

5. Conclusion

Fuzzy logic control of a PV system integrated with an energy storage solution can significantly improve system performance, stability, and adaptability under varying environmental conditions. The FLC effectively manages the nonlinear dynamics of both PV power generation and battery storage, resulting in smoother power delivery, improved energy utilization, and extended battery life. This work showed that, compared to traditional techniques, the FLC approach provided greater flexibility and strength in dealing with uncertainties arising from fluctuations in solar radiation and temperature. However, some limitations have been identified. The design and adjustment of fuzzy inference systems rely heavily on specialized knowledge and empirical rules, which may not guarantee optimal performance on a global scale. Furthermore, the computational complexity of real-time fuzzy processing may increase in large-scale systems or high-precision control tasks. Experimental verification under varying atmospheric conditions and long-term operation remains essential to confirm the system's reliability and long-term scalability.

Future work should focus on integrating adaptive or hybrid FLC strategies such as fuzzy neural predictive control or fuzzy modelling to enable automatic rule modification and learning. Furthermore, integrating real-time monitoring, advanced solar radiation forecasting, and optimal energy scheduling would enhance the efficiency of photovoltaic energy storage systems and support their deployment in smart grids and distributed power networks.

Author Contributions

H.B. conceptualized the study, developed the methodology and software, performed the validation, formal analysis, and investigation, contributed to the resources and data curation, prepared the original draft of the manuscript, reviewed and edited the manuscript, performed the visualization, supervised the research, administered the project, and acquired the funding; Kh. N. Kh. contributed to the conceptualization, software development, validation, investigation, and resources, prepared the original draft of the manuscript, and supervised the research. All authors have read and approved the final version of the manuscript.

Acknowledgements

Not applicable.

Conflict of Interest

The authors declare no conflict of interest.

References

[1] B. Habib, "A comparative study between FSMC and FSOSMC strategy for a DFIG-based wind turbine system," *Majlesi Journal of Mechatronic Systems*, vol. 8, no. 2, 2019.

[2] B. Habib, "36 sectors DTC based on fuzzy logic of sensorless induction motor drives," *Research & Reviews: Journal of Engineering and Technology*, vol. 7, no. 1, pp. 24–31, 2018.

[3] M. H. Ali, T. Murata, and J. Tamura, "A fuzzy logic-controlled superconducting magnetic energy storage for transient stability augmentation," *IEEE Transactions on Control Systems Technology*, vol. 15, no. 1, pp. 144–150, 2007, doi: 10.1109/TCST.2006.883342.

[4] K. Y. Yap, C. M. Beh, and C. R. Sarimuthu, "Fuzzy logic controller-based synchronverter in grid-connected solar power system with adaptive damping factor," *Chinese Journal of Electrical Engineering*, vol. 7, no. 2, pp. 37–49, 2021, doi: 10.23919/CJEE.2021.000014.

[5] M. Mohamed, Z. M. Alaas, B. A. Faiya, H. Y. Hegazy, W. I. Mohamed, and S. A. M. Abdelwahab, "Performance improvement of grid-connected PV-wind hybrid systems using adaptive neuro-fuzzy inference system and fuzzy FOPID advanced control with OPAL-RT," *IEEE Access*, vol. 13, pp. 55996–56020, 2025, doi: 10.1109/ACCESS.2025.3548926.

[6] D. J. Petrović, M. M. Lazić, B. V. Jovanović Lazić, B. D. Blanuša, and S. O. Aleksić, "Hybrid power supply system with fuzzy logic controller: Power control algorithm, main properties, and applications," *Journal of Modern Power Systems and Clean Energy*, vol. 10, no. 4, pp. 923–931, 2022, doi: 10.35833/MPCE.2020.000069.

[7] S. Bergies, C.-L. Su, and M. Elsisi, "New design of robust model predictive control for wind power system using frequency domain bands and dandelion-optimizer," *IEEE Transactions on Reliability*, vol. 74, no. 3, pp. 3718–3729, 2025, doi: 10.1109/TR.2024.3488122.

[8] B. Habib, "Fuzzy second order sliding mode controller based on three-level fuzzy space vector modulation of a DFIG for wind energy conversion systems," *Majlesi Journal of Mechatronic Systems*, vol. 7, no. 3, pp. 17–26, 2018.

[9] B. Habib, "24 sectors DTC control of IM drive using ANFIS controller for minimize torque ripple," *International Journal of Energy and Environment*, vol. 12, pp. 24–29, 2018.

[10] P. Duan, C.-J. Ding, G.-M. Yuan, and M.-L. Zhang, "Wall-following of mobile robot based on fuzzy genetic algorithm to linear interpolating," *Fuzzy Information and Engineering*, vol. 2, no. 2, pp. 201–211, 2010, doi: 10.1007/s12543-010-0045-6.

[11] B. Habib, "Comparison study between FPWM and NSVM inverter in neuro-sliding mode control of reactive and active power control of a DFIG-based wind energy," *Majlesi Journal of Energy Management*, vol. 6, no. 4, 2017.

[12] S.-C. Huang, M.-K. Jiau, and C.-H. Lin, "Optimization of the carpool service problem via a fuzzy-controlled genetic algorithm," *IEEE Transactions on Fuzzy Systems*, vol. 23, no. 5, pp. 1698–1712, 2015, doi: 10.1109/TFUZZ.2014.2374194.

[13] B. Habib, "FPWM technique based based converter for IM drives," *Acta Electrotehnica*, vol. 19, no. 1, pp. 32–41, 2019.

[14] P. Dziwiński and Ł. Bartczuk, "A new hybrid particle swarm optimization and genetic algorithm method controlled by fuzzy logic," *IEEE Transactions on Fuzzy Systems*, vol. 28, no. 6, pp. 1140–1154, 2020, doi: 10.1109/TFUZZ.2019.2957263.

[15] F. Tlili and F. Bacha, "Fuzzy logic direct power control of a bidirectional three-phase AC/DC converter," *2020 20th International Conference on Sciences and Techniques of Automatic Control and Computer Engineering (STA)*, Monastir, Tunisia, pp. 201–206, 2020, doi: 10.1109/STA50679.2020.9329316.

[16] H. Benbouhenni, Z. Boudjema, and A. Belaidi, "DFIG-based wind energy conversion system using five-level FSVM technique," *International Journal of Renewable Energy Technology*, vol. 10, no. 1, 2019.

[17] B. Heber, L. Xu, and Y. Tang, "Fuzzy logic enhanced speed control of an indirect field-oriented induction machine drive," *IEEE Transactions on Power*

Electronics, vol. 12, no. 5, pp. 772–778, 1997, doi: 10.1109/63.622994.

[18] H. Benbouhenni, "Comparative study between PWM and SVPWM technique for a DFIG-based wind turbine system controlled by fuzzy sliding mode," *Majlesi Journal of Energy Management*, vol. 7, no. 4, 2018.

[19] Y. Wang, S. Tang, J. Guo, X. Wang, and C. Liu, "Fuzzy-logic-based fixed-time geometric backstepping control on SO(3) for spacecraft attitude tracking," *IEEE Transactions on Aerospace and Electronic Systems*, vol. 55, no. 6, pp. 2938–2950, 2019, doi: 10.1109/TAES.2019.2896873.

[20] K. Walid, M. Sofiane, B. Habib, G. Hamza, and T. Es-saadi, "Application of third-order sliding mode controller to improve the maximum power point for the photovoltaic system," *Energy Reports*, vol. 9, pp. 5372–5383, 2023, doi: 10.1016/j.egyr.2023.04.366.

[21] N. Debdouche, B. Deffaf, H. Benbouhenni, Z. Laid, and M. I. Mosaad, "Direct power control for three-level multifunctional voltage source inverter of PV systems using a simplified super-twisting algorithm," *Energies*, vol. 16, p. 4103, 2023, doi: 10.3390/en16104103.

[22] N. Debdouche, L. Zarour, B. Habib, F. Mehazzem, and B. Deffaf, "Robust integral backstepping control microgrid connected photovoltaic system with battery energy storage through multi-functional voltage source inverter using direct power control SVM strategies," *Energy Reports*, vol. 10, pp. 565–580, 2023, doi: 10.1016/j.egyr.2023.07.012.

[23] B. Deffaf, H. Farid, B. Habib, S. Medjmadj, and N. Debdouche, "Synergetic control for three-level voltage source inverter-based shunt active power filter to improve power quality," *Energy Reports*, vol. 10, pp. 1013–1027, 2023, doi: 10.1016/j.egyr.2023.07.051.

[24] N. Debdouche, H. Benbouhenni, L. Zarour, F. Mehazzem, B. Deffaf, A. Chebabhi, and T. A. H. Alghamdi, "Nonlinear MPPT techniques to control hybrid power systems," *Scientific Reports*, vol. 14, p. 18620, 2024, doi: 10.1038/s41598-024-69403-6.

[25] A. Belhadj Djilali, A. Yahdou, H. Benbouhenni, and I. Colak, "Improved incremental conductance MPPT technique designed to addressing drift problem in a photovoltaic system," *Electric Power Components and Systems*, pp. 1–14, 2024, doi: 10.1080/15325008.2024.2348040.

[26] N. Debdouche, L. Zarour, A. Chebabhi, N. Bessous, B. Habib, and I. Colak, "Genetic algorithm-super-twisting technique for grid-connected PV system associate with filter," *Energy Reports*, vol. 10, pp. 4231–4252, 2023, doi: 10.1016/j.egyr.2023.10.074.

[27] K. N. Khallouf, Z. Laid, H. Benbouhenni, N. Debdouche, and Z. M. S. Elbarbary, "Adaptive fuzzy logic control for microgrid-connected hybrid photovoltaic/wind generation systems," *Energy Reports*, vol. 12, pp. 4741–4756, 2024, doi: 10.1016/j.egyr.2024.10.042.

[28] F.-Z. Hadjaidji, D. Boukhetala, N. Debdouche, H. Benbouhenni, J.-P. Barbot, and L. Zarour, "Performance evaluation of nonlinear control approaches for grid-connected PV systems includes a novel fractional-order terminal-super twisting approach," *Energy Reports*, vol. 12, pp. 5024–5043, 2024, doi: 10.1016/j.egyr.2024.10.059.

[29] A. Belhadj Djilali, A. Yahdou, E. Bounadja, and H. Benbouhenni, "Fuzzy logic based-perturb and observe control with energy management for photovoltaic-battery and diesel hybrid system," *Arabian Journal for Science and Engineering*, 2024, doi: 10.1007/s13369-024-09348-0.

[30] K. Boutaghane, H. Benbouhenni, N. Bennecib, I. Colak, Z. M. S. Elbarbary, and S. F. Al-Gahtani, "Using new control strategies to improve the effectiveness and efficiency of the hybrid power system based on the battery storage system," *Scientific Reports*, vol. 15, p. 4730, 2025, doi: 10.1038/s41598-025-88804-9.

[31] Z. Sarra, M. Bouziane, R. Bouddou, B. Habib, S. Mekhilef, and Z. M. S. Elbarbary, "Intelligent control of hybrid energy storage system using NARX-RBF neural network techniques for microgrid energy management," *Energy Reports*, vol. 12, pp. 5445–5461, 2024, doi: 10.1016/j.egyr.2024.11.023.

[32] N. Debdouche, H. Benbouhenni, B. Deffaf, G. Anwar, and L. Zarour, "Predictive direct power control with phase-locked loop technique of three-level neutral point clamped inverter-based shunt active power filter for power quality improvement," *International Journal of Circuit Theory and Applications*, vol. 52, no. 7, pp. 3306–3340, 2024, doi: 10.1002/cta.3871.